

RESEARCH ARTICLE

A Novel Global Maximum Power Point Tracking Method Based on Measurement Cells

RODRIGO H. MORALES¹, JAIME A. ROHTEN², (Member, IEEE), MATÍAS N. GARBARINO¹,
JAVIER A. MUÑOZ³, (Member, IEEE), JOSÉ J. SILVA⁴, ESTEBAN S. PULIDO⁵,
JOSE R. ESPINOZA¹, (Senior Member, IEEE), AND MARCOS L. ANDREU⁶

¹Department of Electrical Engineering, Universidad de Concepción, Concepción, Región del Bío-Bío 4070386, Chile

²Department of Electrical and Electronic Engineering, Universidad del Bío-Bío, Bío-Bío, Región del Bío-Bío 4051381, Chile

³Department of Electrical Engineering, Universidad de Talca, Curicó 3340000, Chile

⁴Department of Engineering Science, Universidad de Los Lagos, Puerto Montt 5480000, Chile

⁵Department of Electrical Engineering, Universidad Técnica Federico Santa María, Valparaíso 2390123, Chile

⁶Department of Mining and Geological Engineering, University of Arizona, Tucson, AZ 85721, USA

Corresponding author: Jaime A. Rohten (jrohten@ubiobio.cl)

This work was supported in part by the Chilean Government under Project ANID/FONDECYT/1191028; in part by the Universidad del Bío-Bío under Project 2060119 IF/R; in part by the Renewable Energies and Energy Efficiency Group under Grant 2160180 G/EF-UBB, under Grant ANID/FONDAP/SERC 15110019, under Grant ANID/FONDEQUIP/EQM140148; and in part by the Department of Electrical and Electronic Engineering, Universidad del Bío-Bío.

ABSTRACT Solar power generation has become a solution to mitigate the severe effects on the everyday higher prices of fossil fuels. Additionally, renewable energies operation -as solar- results in a non-polluting way to supply energy, being of special interest into highly contaminated cities and/or countries. The solar energy efficiency injection system is known to be high and mainly due to the power converters effectiveness, which is over of 95% for low and medium voltage. However, this efficiency is reduced when the solar array is partially shaded because traditional maximum power point tracking (MPPT) algorithms are not able to find the maximum power point (MPP) under irregular radiation. This work presents a new algorithm to find the global MPP (GMPP) based upon two MPPTs algorithms used regularly in uniform solar condition (USC), these are the Measuring Cell (MC) and the Perturb and Observe (P&O) methods. The MC ensures to find the surroundings of every local MPP (LMPP) faster and then choose among them the surroundings of the GMPP. Once the surroundings of GMPP are found, the P&O is used to get closer to the GMPP but reducing the DC voltage oscillation to zero hence overcoming the main issue of the P&O. Thus, the proposed algorithm finds the GMPP in two main steps and eliminates the oscillations around the GMPP in steady state, despite the utilization of the P&O. The algorithm is detailed mathematically, illustrated by means of a block diagram, and validated in simulated and experimental results.

INDEX TERMS DC-AC power converter, GMPPT, MPPT, PV system, partial shading algorithm.

I. INTRODUCTION

The introduction of renewables energies (REs) has brought a possibility to release the fossil fuel dependance and reduce the pollution of traditional power sources. Particularly, photovoltaic (PV) solar energy is positioned as one of the most prominent ways to supply energy. In fact, PV is expected to cover 25% (8500 GW) of the world's electricity needs by 2050, representing a 21% (4.9 Gt CO₂) of carbon emissions reduction [1]. The PV are connected into the grid through

The associate editor coordinating the review of this manuscript and approving it for publication was Chi-Seng Lam¹.

a power converter, in charge of the maximum power point tracking (MPPT) algorithm, while the solar system can work in different weather conditions *i.e.* different radiation and temperature [2]. In order to operate effectively under variable weather conditions, while harvesting the maximum possible power at any time, a suitable maximum power point tracking (MPPT) algorithm must be included to operate the power converter in the maximum power point (MPP) and, therefore, improve the system total efficiency [3]. On the other hand, some installations are under the possibility to be partially shaded and the main problem associated to this issue is the pop up of more than one local MPP (LMPP) [4], [5],

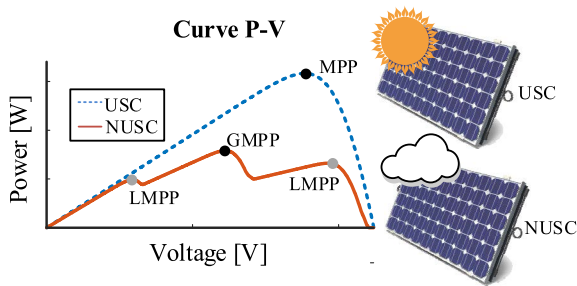


FIGURE 1. Curve P-V under uniform solar condition (USC) and non-uniform solar condition (NUSC) for PV array.

leading to traditional MPPT algorithms to miss the global MPP (GMPP). The MPPT algorithms can be divided into two broad categories: *i*) MPPT algorithms for ideal systems or without shading, *i.e.*, under uniform solar condition (USC) [6] and *ii*) MPPT algorithms for systems under partial shading, *i.e.*, non-uniform solar condition (NUSC), also named partial shading condition (PSC) [7], [8]. FIGURE 1 illustrates that USC causes a single MPP, while PSC or NUSC may cause multiple LMPP.

The most widely used conventional algorithms are the perturb and observe (P&O), and incremental conductance (INC) [3]. In addition, there are some other algorithms derived from the P&O and INC for USC, where the power $p(k)$ is compared with previous power $p(k - 1)$ to later decide to increase or decrease the voltage-step to reach the MPP by employing an AC-DC [9] or DC-DC [10] converter. All of these algorithms do not guarantee to find the GMPP for systems under PSC [3]. Indeed, these algorithms must be modified or a more complex algorithm such as those presented in [4], [11], [12], [13], [14], [15], [16], and [17] must be implemented to obtain the GMPP. One of the ways to obtain the GMPP for systems under PSC is to perform a sweep (scan) of the power-voltage (P-V) curve to determine the GMPP [16], [18]. On the other hand, [5] presents a review of ten different hybrid algorithms to obtain the GMPP, some of them are based on conventional algorithms such as P&O and INC, others are based on more complex algorithms such as gray wolf optimization (GWO), particle swarm optimization (PSO), artificial neural network (ANN), among others. Each algorithm has advantages and disadvantages, such as efficiency and tracking time (scan period). For example, in [17] the authors present a “hybrid global MPPT (GMPPT)” based on hill climbing (HC) and artificial bee colony (ABC) algorithms, they also use a boost converter, a battery, and an inverter to obtain the simulation results showing an efficiency close to 99%, and tracking time of 0.26s and 1.3s for USC and PSC, respectively. In [16] the authors present a “high-speed MPPT module” algorithm, they also use a boost converter to obtain simulation results, this algorithm has an efficiency of 99.98%, tracking time of 0.022s and 0.034s for USC and PSC, respectively.

On the other hand, in [19], [20], and [21] the MPPT is obtained through an algorithm that does not use the

P-V curve to determine the next step. This algorithm is based on the equations that model a photovoltaic cell, so it uses two measurement cells, one in short-circuit (SC) to obtain the current i_{sc} , and another in open-circuit (OC) to obtain the voltage v_{oc} , to compute the internal variables and therefore estimate the MPP. However, these algorithms were not designed for PSC, but they are faster than conventional algorithms (P&O and INC), which is of particular interest to improve the efficiency.

After obtaining the MPPT or GMPPT, to be able to make use of the solar PV energy, it is necessary to use a DC-AC power converter (inverter) to inject the power into the electrical grid. There are different topologies, but one of the most widely used is the three-phase voltage source converter (VSC), because of its simplicity of implementation and control [2], [22], [23], [24], [25]. Typically, in a PV system there are two ways to implement the power injection (*i*) including a DC-DC converter and the DC-AC inverter, which may pump up (or down) the voltage from the PV system to the DC-link, if necessary, and (*ii*) use a simpler scheme, including the DC-link and the DC-AC inverter, for connecting it to the grid. Despite the first one gives more versatile to both amplify or reduce the voltage from the solar system value, it adds more losses because of the additional stage. On the other hand, the second option is employed in larger power systems where the PV array is designed in order to be managed directly by the inverter [2], [3]. In fact, [2] states that power levels over 50 MW should use single a stage DC-AC inverter, instead, if the power level is below 50 kW, states to include the DC-DC stage, and between the abovementioned values states that can be either and must be studied case by case.

This paper proposes a novel GMPPT algorithm based on the measurement cells (MC) algorithm, [19], [20], [21], and the P&O. The proposal is separated in two main steps. The first step is to find all the LMPP surroundings by using the fast dynamic MC algorithm and decide which one has the maximum power, given as a result the one which is closer to the GMPP. Then, in the second step, the P&O approximates the voltage to reach the MPP. The P&O is slightly modified in order to find the GMPP but avoiding the oscillation around the GMPP, as it usually does. Once the P&O algorithm detects that is close to the GMPP, it starts to reduce the voltage-step down to zero, avoiding the undesirable steady state effects of the voltage oscillation. Thus, the DC link voltage reference is given in order to get the MPP independent if the solar array is under USC or NUSC. It is important to highlight that this algorithm holds the advantages of each algorithm, as the fast dynamic of the MC and the robustness of the P&O. Once the algorithm finds the GMPP, the power is constantly computed and if sees an important variation, the GMPPT starts all over again. Thus, in steady state the proposed GMPPT guarantees a non-oscillating voltage and therefore the currents and voltage THD are not affected by this issue.

The currents of the power converter are controlled by a nonlinear law and the DC link voltage loop is based on the

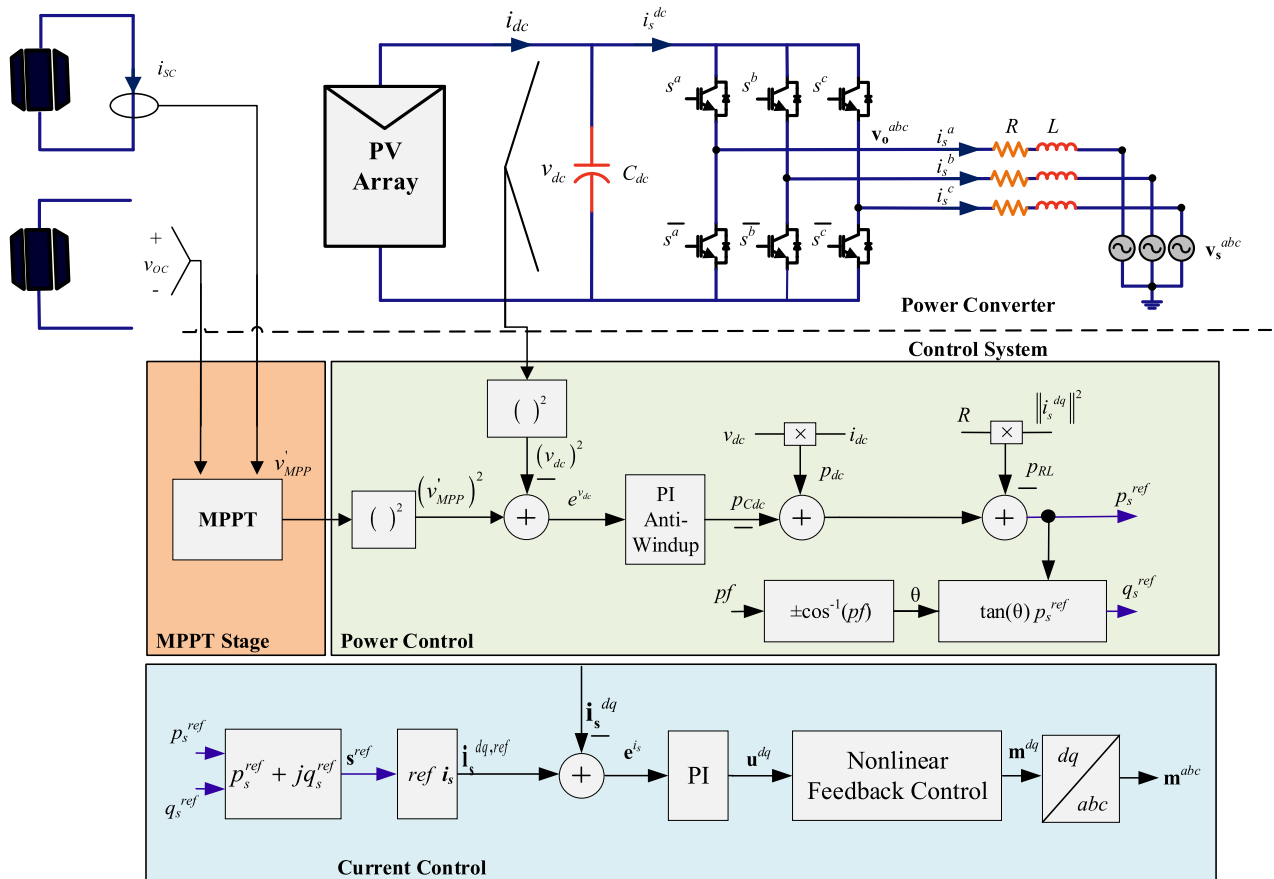


FIGURE 2. Diagram of control and system topology.

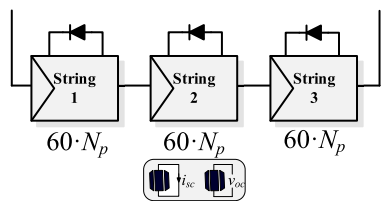


FIGURE 3. PV array to simulate.

actual power, allowing to only use a standard Proportional-Integral (PI) controller. The whole system is tested under different weather conditions (different temperature and irradiance) by means of simulated and experimental ways. The results corroborate the control strategy performance and key waveforms to show details of the total behavior are given.

II. PARAMETERS AND PV SYSTEM MODEL

The proposed system, FIGURE 2, contains measurement cells to obtain the GMPPT, a PV array, and a Three-Phase VSC to inject energy into the grid.

The solar array, FIGURE 3, is composed of three series strings of 20 PV panels each string (and two measurement cells). This configuration is chosen to simulate the

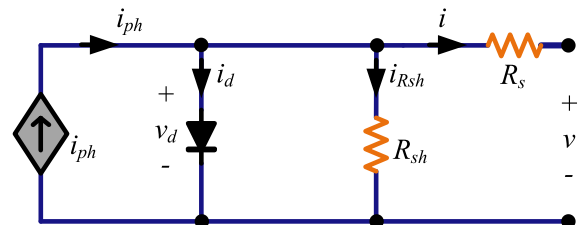


FIGURE 4. Equivalent circuit of solar cell.

“RISEN RSM60-6-265P” (RSM265) panel which contains 60 cells in series. The parameters of the solar array are listed in TABLE 1.

A. SOLAR CELL MODEL

A PV array is a set of cells organized in series and parallel that can be represented with a circuit model as illustrated in FIGURE 4. The solar cell is modeled by a current source, which represents the solar irradiance; one diode, representing the $p-n$ semiconductor junction; two resistances, one in parallel to the diode and other in series with the load, which represent the solar module internal losses. The cell’s mathematical model is obtained by applying Kirchhoff’s laws, and it can be found that:

$$i = i_{ph} - i_d - i_{Rsh}, \quad (1)$$

TABLE 1. Parameters solar system.

Parameters		Value
PV Array	Power max	15.9 [kW]
	Open Circuit Voltage max	2280 [V]
	Short Circuit Current max	9.12 [A]
	Strings	3
	Panels by strings	20
	Cells by panel	60
PV Panel	Power max p_{MPP}	265 [W]
	Open Circuit Voltage v_{oc}	38 [V]
	Short Circuit Current i_{sc}	9.12 [A]
	Maximum Power Voltage v_{MPP}	30.9 [V]
	Maximum Power Current i_{MPP}	8.58 [A]
PV Cell (Simulation)	Series Resistance R_s	0.0079 [Ω]
	Shunt Resistance R_{sh}	1000 [Ω]
	Short Circuit Current i_{sc0} at USC	3.8 [A]
	Diode Saturation Current i_0	$1.12 \cdot 10^{-8}$ [A]
	Band Energy E_g	1.12 [eV]
	Ideality Factor n	1.2
	Ref. Temperature T_{ref}	298 [K]

where i is the current obtained from PV cell, i_{ph} represents the current due to the solar irradiance, i_{Rsh} is associated to the R_{sh} power losses (diode losses), and i_d represents the diode intrinsic current, and is expressed in the form of the Shockley diode equation:

$$i_d = i_0 \left(\exp \left(\frac{qv_d}{nkT} \right) - 1 \right), \quad (2)$$

with,

- i_0 : Diode saturation inverse current.
- v_d : Diode voltage.
- k : Boltzmann constant ($1.381 \cdot 10^{-23}$ [J/K]).
- T : Absolute temperature in Kelvin [K].
- n : Diode ideality factor.
- q : Electron charge ($1.6 \cdot 10^{-19}$ [C]).

Replacing (2) in (1),

$$i = i_{ph} - i_0 \left(\exp \left(\frac{qv_d}{nkT} \right) - 1 \right) - i_{Rsh}. \quad (3)$$

On the other hand, the current i_{Rsh} and the diode voltage v_d can be rewritten as $i_{Rsh} = v_d/R_{sh}$ and $v_d = v + iR_s$, where R_s is the series resistance representing the conducting power losses. Therefore, the output current cell is:

$$i = i_{ph} - i_0 \left(\exp \left(\frac{q(v + iR_s)}{nkT} \right) - 1 \right) - \frac{v + iR_s}{R_{sh}}. \quad (4)$$

B. MODEL AND CONVERTER CONTROL

To inject the energy from a solar system into the grid, it is necessary to use a power inverter. In this case, a Three-Phase VSC, as shown in FIGURE 2, is used. The equations that model the converter are as follows:

$$\begin{aligned} \mathbf{v}_o^{abc} &= \mathbf{R}\mathbf{i}_s^{abc} + L \frac{d\mathbf{i}_s^{abc}}{dt} + \mathbf{v}_s^{abc} \\ C_{dc} \frac{dv_{dc}}{dt} &= i_{dc} - i_s^{dc}, \end{aligned} \quad (5)$$

where for the average model $\mathbf{v}_o^{abc} = G_{ac}\mathbf{m}_s^{dq}v_{dc}$ (G_{ac} is the modulation gain and \mathbf{m}_s^{dq} the modulating signals) represents the injected voltage by the VSC, \mathbf{i}_s^{abc} is the injected current, \mathbf{v}_s^{abc} is the grid voltage, which is considered as a disturbance for control purposes, v_{dc} is the DC-link voltage, i_{dc} is the solar PV current, i_s^{dc} is the DC side current of the power converter, and C_{dc} , R , L are the power converter filter parameters.

The power converter control can be separated into 1) power control and 2) current control. Note that despite a two-levels inverter is used, the proposal can be extended to any topology, updating only the current control with the new switching pattern according to the topology to track the current reference.

1) POWER CONTROL

The power control can be divided into *i*) the energy stored by the DC-link capacitor (associated to the power p_{Cdc}), *ii*) the power provided by the solar array (p_{dc}), and *iii*) the inductive filter power losses (p_{RL}) [26].

The energy stored or supplied by the capacitor is associated with the power as:

$$p_{Cdc} = \frac{1}{2}C_{dc} \frac{d(v_{dc})^2}{dt}. \quad (6)$$

The power provided by the solar array:

$$p_{dc} = v_{dc} \cdot i_{dc}, \quad (7)$$

where $p_{dc} = p_{pv}$ represents the DC power is supplied by the solar array, $v_{dc} = v_{PV}$ is the solar array PV voltage, and $i_{dc} = i_{PV}$ is the solar array PV current.

The power losses at the AC RL filter are defined as:

$$p_{RL} = \left\| \mathbf{i}_s^{dq} \right\|^2 R. \quad (8)$$

Thus, the total power delivered into the grid follows the relation:

$$p_s^{ref} = p_{dc} - p_{RL} - p_{Cdc}, \quad (9)$$

where p_s^{ref} represents the active power reference to be injected into the grid.

From (9) it can be seen that the only controllable power is p_{Cdc} , therefore, a PI Anti-Windup controller is used to regulate this power and, thus, avoid the cumulated error that a PI controller has if the system is saturated. Also, the DC voltage reference is given by the MPPT algorithm ($v_{dc}^{ref} = v'_{MPP}$) which is to be followed by the DC-link voltage control, where v'_{MPP} is explained in section IV. The discrete transfer function of the PI control used is:

$$h_{PI}^{v_{dc}}(z) = k_c^{v_{dc}} \frac{k_1^{v_{dc}} + k_2^{v_{dc}}z^{-1}}{1 - z^{-1}}, \quad (10)$$

being the power to track the DC-link voltage reference as:

$$p_{Cdc}(k) = p_{Cdc}(k-1) + k_c^{v_{dc}} \left[k_1^{v_{dc}} e^{v_{dc}}(k) + k_2^{v_{dc}} e^{v_{dc}}(k-1) \right], \quad (11)$$

where $e^{v_{dc}}(k) = (v'_{MPP}(k))^2 - (v_{dc}(k))^2$, $k_c^{v_{dc}}$ is the DC voltage control loop gain, $k_1^{v_{dc}}$ and $k_2^{v_{dc}}$ are defined as a

function of the sampling time (T_s) and integrative time (T_i^{vdc}) as:

$$k_1^{vdc} = \left(1 + \frac{T_s}{2T_i^{vdc}}\right), k_2^{vdc} = \left(-1 + \frac{T_s}{2T_i^{vdc}}\right). \quad (12)$$

However, to mitigate the over-integration problems when the controller output is saturated, [27], [28], [29], the PI integrative part must be set to zero, i.e., $I = 1/T_i^{vdc} = 0$, and therefore $k_1^{vdc} = 1$ and $k_2^{vdc} = -1$.

As the active power is already defined, the reactive power (q_s) can be set as a function of the desired power factor (pf) as follow:

$$q_s = \tan(\theta)p_s^{ref} = \tan(\pm \cos^{-1}(pf))p_s^{ref}, \quad (13)$$

where $pf = \cos(\theta)$ represents the power factor. Thus, the total amount of power is defined as:

$$\vec{s}_{pq} = p_s + jq_s, \quad (14)$$

and the currents references are settled to be:

$$i_s^{d,ref} = p_s/v_s^d, \quad (15)$$

$$i_s^{q,ref} = -q_s/v_s^d. \quad (16)$$

2) CURRENT CONTROL

The current control is based on the power converter model, defined in (5), and solving for $d\mathbf{i}_s^{dq}/dt$:

$$\frac{di_s^d}{dt} = \frac{1}{L}G_{ac}m_s^d v_{dc} - \frac{R}{L}i_s^d + \omega i_s^q - \frac{v_s^d}{L}, \quad (17)$$

$$\frac{di_s^q}{dt} = \frac{1}{L}G_{ac}m_s^q v_{dc} - \frac{R}{L}i_s^q - \omega i_s^d - \frac{v_s^q}{L}, \quad (18)$$

where ω is grid angular frequency.

The exact linearization method uses the state variable model to find a nonlinear law that permits a linear behavior between a new input and the output variable. Thus, two new inputs are defined, u^d and u^q , in order to control the two outputs i_s^d and i_s^q . This method is detailed in [30] and [31] showing that not only linearizes the input/output system but also decouples the states variables (currents) in the entire operating region. In addition, this method results simple and easy to implement on digital boards with low computational cost.

The power converter equations are employed in the definition of the nonlinear feedback law, where two new input variables, u^d and u^q , are defined to get a linear relationship between \mathbf{u}^{dq} and derivate of \mathbf{i}_s^{dq} , such that:

$$u^d = \frac{di_s^d}{dt}, \quad u^q = \frac{di_s^q}{dt}. \quad (19)$$

Thus, the modulating signals (\mathbf{m}_s^{dq}) to get a linear behavior can be found from the model in (17)-(18) and the new inputs u^d and u^q as:

$$m_s^d = \frac{1}{G_{ac}v_{dc}} \left(Lu^d + Ri_s^d - L\omega i_s^q + v_s^d \right), \quad (20)$$

$$m_s^q = \frac{1}{G_{ac}v_{dc}} \left(Lu^q + Ri_s^q + L\omega i_s^d + v_s^q \right). \quad (21)$$

Once the nonlinear feedback is defined, the current i_s^d and i_s^q can be controlled independently, considering no coupling between them and no interaction with disturbances as the grid voltage, the solar power variation, among others [32]. To track the current reference, it is recommended to include a PI controller to mitigate the effects of minors errors in the nonlinear feedback of (20) and (21) such as deviation on the parameters, as stated in [30], and non-modeled dynamics, where the PI defines the new input \mathbf{u}^{dq} as:

$$\mathbf{u}^{dq}(k) = \mathbf{u}^{dq}(k-1) + k_c^{is} \left[k_1^{is} \mathbf{e}^{is}(k) + k_2^{is} \mathbf{e}^{is}(k-1) \right], \quad (22)$$

where $\mathbf{e}^{is}(k) = \mathbf{i}_s^{dq,ref}(k) - \mathbf{i}_s^{dq}(k)$, with k_c^{is} the current control loop gain, and k_1^{is} and k_2^{is} are defined in function of the sampling time (T_s) and the current integrative time (T_i^{is}):

$$k_1^{is} = \left(1 + \frac{T_s}{2T_i^{is}}\right), \quad k_2^{is} = \left(-1 + \frac{T_s}{2T_i^{is}}\right). \quad (23)$$

III. MPPT WITH UNIFORM SOLAR CONDITION

The solar PV system depends on the temperature and irradiance, in addition, the PV cells show a nonlinear behavior as seen in FIGURE 1. There are a great variety of MPPT algorithms, all of these keep the system at the MPP, the most employed algorithms are the P&O and INC algorithm [3], [5], but there are several variations of these algorithms. One additional algorithm has been introduced based on measurement cells [19], [21]. However, these algorithms have been reported to be used in USC only, since they are not able to find the GMPP for PSC.

A. MEASUREMENT CELLS ALGORITHM

The MC algorithm is a strategy based on the PV cell mathematical model and on the tracking the MPP employing two measuring PV cells: one single cell in open circuit, to supply the actual open circuit voltage (v_{oc}); and the second cell in short circuit, to supply the short circuit current (i_{sc}). If no single cell is available, a whole solar panel can be employed to find v_{oc} and i_{sc} , as mentioned in the experimental results (section V.B). The above in combination with an integrative (I) control strategy for a fast estimation of the MPP voltage (v_{MPP}) is presented in the following.

1) OPEN CIRCUIT AND SHORT CIRCUIT ANALYSIS

Analyzing the cell PV (FIGURE 4) in open circuit, and assuming $R_s \rightarrow 0$, this entails $v = v_{oc} = v_d$, leaving the current as:

$$i_{ph} = i_d + i_{Rsh}, \quad (24)$$

where $i_{Rsh} = v_{oc}/R_{sh}$, and $i_{ph} = i_{sc}$ considering the cell PV in short circuit, the equation (24) remains:

$$i_{sc} = i_d + \frac{v_{oc}}{R_{sh}}, \quad (25)$$

solving for i_d , considering (2) and $v_d = v_{oc}$, the equation (25) remains:

$$i_d = i_o \left(\exp\left(\frac{qv_{oc}}{nkT}\right) - 1 \right) = i_{sc} - \frac{v_{oc}}{R_{sh}}, \quad (26)$$

then, from (26), and applying properties to solve for v_{oc} , is obtained:

$$v_{oc} = \frac{nkT}{q} \ln \left(\frac{i_{sc}}{i_0} - \frac{v_{oc}}{i_0 \cdot R_{sh}} + 1 \right). \quad (27)$$

Finally, assuming that the parallel resistance is much greater than zero, $R_{sh} \gg 0$, getting that $v_{oc}/(i_0 R_{sh}) \rightarrow 0$, so the estimation of v_{oc} (\hat{v}_{oc1}) in function of temperature (T) and short circuit current (i_{sc}), is defined as:

$$\hat{v}_{oc1} = \frac{nk\hat{T}}{q} \ln \left(\frac{i_{sc}}{i_0} + 1 \right). \quad (28)$$

On the other hand, the diode saturation inverse current should not be taken as a constant value and this nonlinearity must be included in the variable's estimation, where this current can be expressed as a function of the temperature as:

$$i_0 = I_0 \left(\frac{T}{T_{ref}} \right)^3 \exp \left(\frac{qE_g}{nk} \left(\frac{1}{T_{ref}} - \frac{1}{T} \right) \right). \quad (29)$$

where I_0 is the diode saturation current of each solar cell at the reference temperature T_{ref} ; T_{ref} is the temperature under the standard test conditions; and E_g is the band energy of each solar cell, in eV.

2) MAXIMUM POWER POINT ANALYSIS

FIGURE 1 shows the power as a function of the voltage, where the MPP is located where the derivative of the delivered power is equal to zero, moreover, the power is determined as $p = v \cdot i$, therefore the derivative of the power concerning the voltage is:

$$\frac{\partial p}{\partial v} = i + v \frac{\partial i}{\partial v} \Big|_{\substack{i=i_{MPP} \\ v=v_{MPP}}} = 0, \quad (30)$$

solving to find the MPP voltage (v_{MPP}), it is found:

$$v_{MPP} = - \frac{i}{\partial i / \partial v} \Big|_{\substack{i=i_{MPP} \\ v=v_{MPP}}}, \quad (31)$$

where the partial derivate of (4) is:

$$\frac{\partial i}{\partial v} \Big|_{\substack{i=i_{MPP} \\ v=v_{MPP}}} = - \frac{i_0 q}{nkT} \exp \left(q \frac{v + iR_s}{nkT} \right) - \frac{1}{R_{sh}}, \quad (32)$$

replacing (4) in (31), and considering $i_{ph} = i_{sc}$ the v_{MPP} is:

$$v_{MPP} = - \frac{i_{sc} - i_0 \left(\exp \left(\frac{q(v+iR_s)}{nkT} \right) - 1 \right) - \frac{v+iR_s}{R_{sh}}}{- \frac{i_0 q}{nkT} \exp \left(q \frac{v+iR_s}{nkT} \right) - \frac{1}{R_{sh}}} \Big|_{\substack{i=i_{MPP} \\ v=v_{MPP}}}, \quad (33)$$

Solving for (33) and considering $R_{sh} \gg 0$ the voltage v_{MPP} can be found as:

$$v_{MPP} = \frac{nkT}{q} \ln \left(\frac{i_{sc}}{i_0} + 1 \right) - \frac{nkT}{q} \ln \left(v_{MPP} \frac{q}{nkT} + 1 \right) - i_{MPP} R_s \quad (34)$$

considering (28) in (34) is obtained:

$$v_{MPP} = \hat{v}_{oc1} - \frac{nkT}{q} \ln \left(v_{MPP} \frac{q}{nkT} + 1 \right) - i_{MPP} R_s, \quad (35)$$

Finally, the open circuit voltage, analyzing the MPP can be defined alternatively in function of T , v_{MPP} , and i_{MPP} as:

$$\hat{v}_{oc2} = v_{MPP} + \frac{nk\hat{T}}{q} \ln \left(v_{MPP} \frac{q}{nk\hat{T}} + 1 \right) + i_{MPP} R_s. \quad (36)$$

3) MAXIMUM POWER POINT TRACKING

The measurement cells algorithm is based on the cell mathematical model, employing the sensed values from an open circuit cell (the voltage v_{oc}) and a short-circuited cell (the short circuit current i_{sc}). Then, employing (28) and (36) the MPP voltage (v_{MPP}) is estimated.

The temperature has a strong influence on the open circuit voltage v_{oc} , as it can be seen from (28). In addition, despite that (28) shows a nonlinear relationship, in the expected range of temperature, the behavior in FIGURE 5 (a) is closed to linear, moreover, the relationship between the estimation of v_{oc} and T is inversely proportional. On the other hand, analyzing (36), it is also found a linear and direct relationship between v_{oc} and v_{MPP} , as illustrated in FIGURE 5 (b).

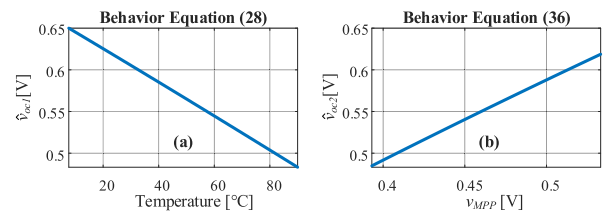


FIGURE 5. Open circuit voltage behavior. (a) as a function of temperature-dependent, (b) as a function of maximum power point voltage.

On the other hand, it is required to solve these equations ((28) and (36)) to estimate the v_{MPP} and T , thus, these values are determined from two Integrative (I) controllers. The first I-controller is set to estimate the T required in (28) that results from the sensed value of v_{oc} and its estimated \hat{v}_{oc1} , as follows:

$$\hat{T}(k) = \hat{T}(k-1) + \frac{T_s}{2T_i^1} \left[e^1(k) + e^1(k-1) \right], \quad (37)$$

where $e^1(k)$ is the error between sensed value of v_{oc} and its estimated \hat{v}_{oc1} from (28), and T_i^1 is the controller negative gain integrative time -due to the inversely proportional behavior of this relationship FIGURE 5 (a)-.

The second I-controller is used to determine the v_{MPP} from (36), that results from the estimated value \hat{v}_{oc2} , as follows:

$$v_{MPP}(k) = v_{MPP}(k-1) + \frac{T_s}{2T_i^2} \left[e^2(k) + e^2(k-1) \right], \quad (38)$$

where $e^2(k)$ is the error between sensed v_{oc} and its estimated \hat{v}_{oc2} from (36) and T_i^2 is the controller gain integrative time.

The implementation of both controllers is illustrated in FIGURE 6, where the temperature and the v_{MPP} are part of the control loops. Moreover, the measuring cells provide the actual values of the current i_{sc} and the actual voltage v_{oc} required by this estimator to find the v_{MPP} , considering all nonlinearities of the solar cell. This algorithm performs the MPPT without oscillations in comparison with other algorithms [3], [21], [34]. On the other hand, the current i_{MPP} is equal to the i_{dc} measurement of the system (when the system is in the MPP, $i_{dc} = i_{MPP}$)

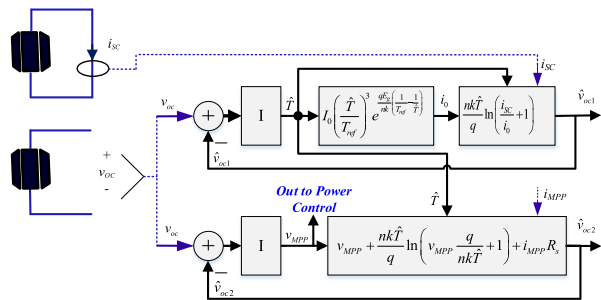


FIGURE 6. Block diagram of measurement cells MPPT.

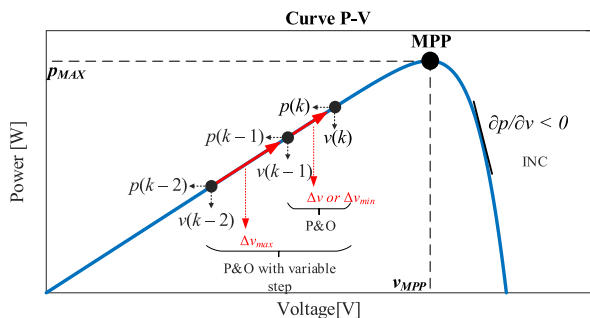


FIGURE 7. Behavior conventional algorithms: P&O uses fixed Δv , P&O with variable step uses Δv_{min} and Δv_{max} , and INC uses tangent of the curve.

Therefore, as a result, this algorithm gives the MPP voltage, which is the main objective, and also, the semiconductor junction temperature (required to find the MPP), which is not easy to measure, and it does not correspond to the weather temperature.

B. CONVENTIONAL ALGORITHMS

The conventional MPPT algorithms most used are the P&O and INC, as well as their derivations [3], [5]. These algorithms are very similar and based in the DC-link capacitor voltage modification (increasing or decreasing it). The P&O algorithm uses the actual power $p(k)$ to compare if it is greater or lesser than the previous power $p(k - 1)$, likewise, the actual and previous voltage are analyzed, to decide if either increase or decrease this voltage named Δv . The INC algorithm uses the curve slope (curve tangent) to decide whether to increase or decrease the voltage, if the slope is positive, the voltage is increased, otherwise, the voltage is decreased, but if the slope

is zero, the voltage is kept constant. An improvement on the P&O algorithm is to vary the step Δv length, this algorithm is named P&O of variable step (P&O-VS), defining an Δv_{max} depending how far the algorithm is from the MPP, and therefore, after being close to the MPP the step is decreased to Δv_{min} to also decrease the oscillations around this point. The progression of each MPPT is illustrated in FIGURE 7.

C. COMPARISON MPPT ALGORITHMS WITH USC

FIGURE 8 presents a comparison of these techniques (P&O, P&O-VS, INC, MC) tracking the MPP in an array of 34 PV panels, with a power around 6kW for 700W/m² and 25°C. The temperature was reduced from 25 to 20°C at 0.1[s]. Simulations of the conventional MPPT algorithms are performed considering $\Delta v = 5V$. In FIGURE 8 (a) the MPPT of each algorithm is observed, where the MC algorithm (p_{cells}) is the fastest, reaching the MPP in about 30ms, whereas the conventional algorithms have a tracking time of about 62ms, however, the conventional algorithms can be faster, increasing voltage variation (Δv), but, this will cause a greater oscillation on the voltage reference because $v_{dc}^{ref} = v_{MPP}$, as presented in FIGURE 8 (b). On the other hand, the MC based algorithm has no oscillations in the MPP, also the energy between 0.1s – 0.25s is 36.554kW for the MC algorithm, and of 36.545kW for the other algorithms. The comparison was made considering the whole system shown in FIGURE 2, which includes the MPPT, converter DC-AC, inductive filter and grid source, and a sampling time $T_s = 100\mu s$ for the MPPT algorithms.

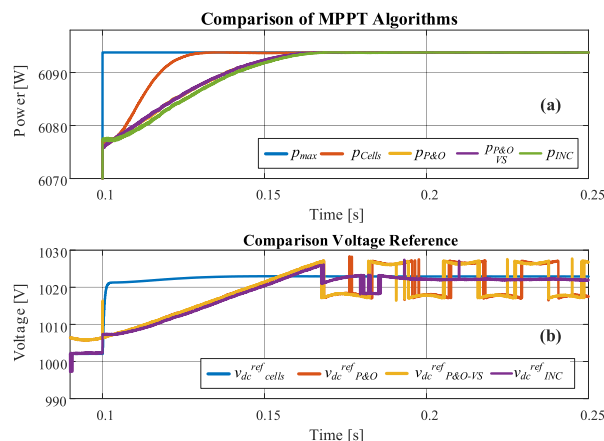


FIGURE 8. Comparison MPPT's Algorithms for uniform solar condition (USC). (a) MPP (power) comparison, (b) voltage variation comparison.

IV. PROPOSED MPPT WITH PARTIAL SHADING CONDITION

In this section, the proposed algorithm for PV systems with Partial Shading Condition (PSC) is presented. The proposed algorithm is composed by a combination of two previous algorithm: the MC and P&O with variable step (P&O-VS), extended to find the global MPP (GMPP). The MC is used to rapidly determine the voltage in the GMPP neighborhood, and the P&O to get the closest to the GMPP.

The MC algorithm estimates the v_{MPP} from the measuring cells, independent of the PV array shade, since the v_{MPP} determined by this algorithm depends on the irradiance and temperature on the cells. Ideally, the measurement cells are expected to be in an unshaded location to obtain the v_{MPP} , in case of shading, the v_{MPP} determined will be incorrect, so the modified P&O-VS algorithm finds the correct v_{MPP} , as it will be explained later. It is possible to use only two measurement cells for all strings or two measurement cells for each string; in the first case, the v_{oc} and i_{sc} measured by the cells are considered to determine the v_{MPP} , in the second case, the v_{oc} and i_{sc} of each pair of measurement cells are analyzed and the highest v_{oc} and i_{sc} is selected to determine the v_{MPP} .

As explained before (FIGURE 6), in the MC algorithm the first controller estimates the temperature, and the second controller determines the v_{MPP} . These measurements are obtained only from a single PV cell; therefore, this value must be amplified by considering the number of cells in the PV array. For example, in a PV array of 20 panels, where each panel contains 60 cells (TABLE 1), the final MPP voltage is $v'_{MPP} = 60 \times 20 \times v_{MPP}$, and this voltage is applied to the entire array, and therefore every string, panel or cell may have different voltages among them. This result can be generalized according to (39).

$$v'_{MPP} = N_c \cdot N_p \cdot v_{MPP}, \tag{39}$$

where v'_{MPP} is the final MPP voltage, N_c is the number of cells contained in the PV panel, and N_p is the number of panels in series in the PV array.

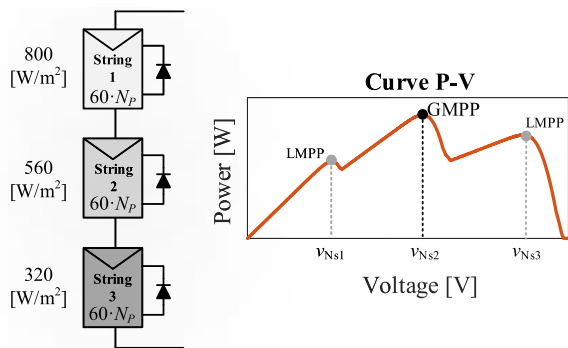


FIGURE 9. Example of PV system divided by string.

However, a large PV array can be divided in strings, as presented in FIGURE 9, so the equation (39) is rewritten as:

$$v'_{MPP} = N_c \cdot N_p \cdot N_s \cdot v_{MPP} \tag{40}$$

where N_s is the number of strings of the large-scale PV array.

Without losing generality, it is considered a partial shading relationship as presented in FIGURE 9, with three strings of 60 PV panels each one, with an irradiance of 800W/m^2 , 560W/m^2 , and 320W/m^2 respectively, all of them with a temperature of 25°C , it is obtained a P-V curve with three

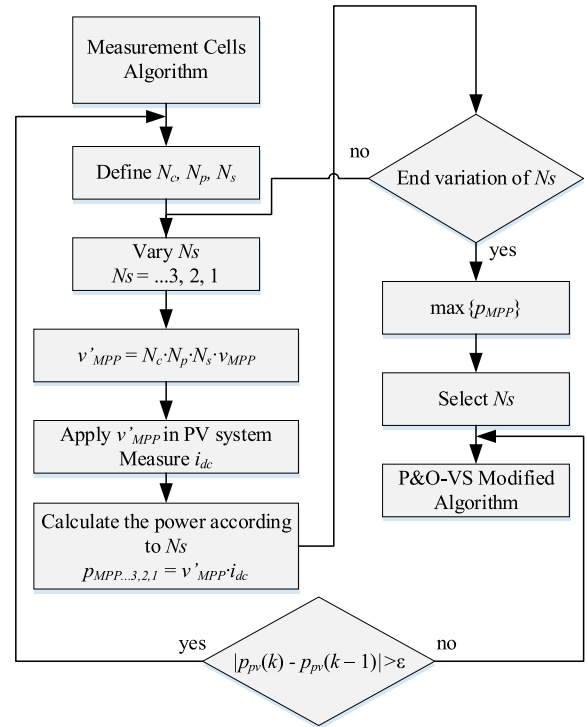


FIGURE 10. Proposed partial shading algorithm.

peaks (LMPP-GMPP-LMPP). The MPP will be always associated to one of these peaks and, therefore, the v'_{MPP} can be determined considering any of the N_s possibilities, i.e.: $N_s = 3$, $N_s = 2$, or $N_s = 1$, leading to choose the voltages: v_{Ns3} , v_{Ns2} , or v_{Ns1} . In the case of FIGURE 9, the GMPP is around $N_s = 2$ (v_{Ns2}). Hence, the MC algorithm rapidly finds the surroundings of the MPP, testing $N_s = 3, 2, 1$, and saving the power at each to the tests ($P_{MPP...3,2,1} = v'_{MPP...3,2,1} \cdot i_{dc}$), finally to secure the MPP or GMPP a modified P&O-VS algorithm is used.

The proposed algorithm is presented in the block diagram of FIGURE 10. After the v_{MPP} is determined by the MC algorithm, it determines the v'_{MPP} , with the N_s value associated to the greater power by testing with $N_s = N_T, \dots, 3, 2, 1$, where N_T is the total number of strings. Once the N_s values tests are finished, the P&O takes place to proximate more to the global MPP (GMPP). This P&O algorithm is modified to a variable step (modified P&O-VS). The variable step goes from a given Δv till reach zero by means of $\Delta v = \Delta v - \delta v$, avoiding oscillations around the MPP in steady state.

FIGURE 11 presents the diagram of the modified P&O-VS algorithm, this algorithm uses a new variable $v'(k)$, which is in charge to save only the variations of Δv with the initial value given by $v'(0) = 0$, independent of the actual voltage $v_{dc}(k)$ contaminated by noise, because $v(k+1) = v_{dc}(k) \pm \Delta v$. The voltage variation Δv depends on ΔMin and is updated each time the algorithm oscillates around the MPP until a $\Delta v = 0$ is obtained, as explained below.

When $v'(k) = v'(k-2)$ indicates the MPP voltage reference has returned to its initial path and therefore is presumably

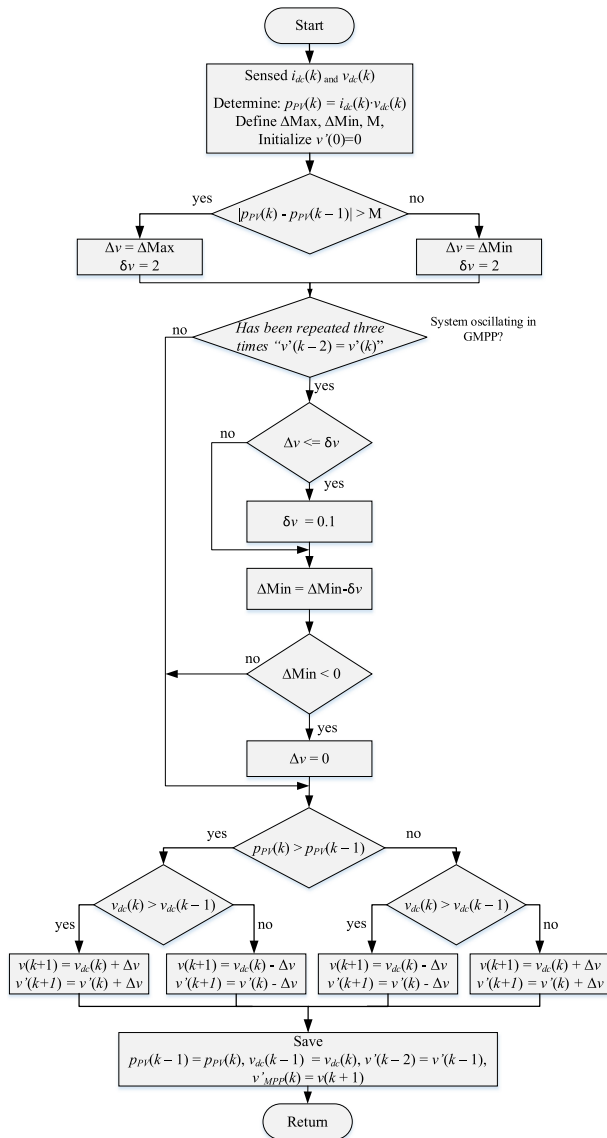


FIGURE 11. Proposed perturb and observe with variable step modified algorithm to eliminate oscillation (P&O-VS modified).

close to the MPP. To avoid the noise effect on this algorithm, if $v'(k) = v'(k - 2)$ occurs three times it is said the MPP is close and then Δv is decreased for a better approximation to the MPP by summing $-\delta v$ to ΔMin ($\Delta Min = \Delta Min - \delta v$), for this case $\Delta Max = 20V$ and $\Delta Min = 10V$. When the value of Δv is low ($\Delta v = \delta v$) the value of δv is decreased to $\delta v = 0.1$. When $\Delta Min < 0$, the value of Δv is forced to be zero, finding the GMPTT. The values ΔMax , ΔMin , δv depend on the PV system, it is recommended to define the values such that ΔMax is around 1% of the system voltage, ΔMin is half of ΔMax , and δv is 10% of ΔMax .

Once the GMPP is found, the proposed algorithm will stay in that point until it detects variations on the power. In other words, the algorithm wakes up when there is a change in power, which is analyzed by the variation of power given by $|p_{PV}(k) - p_{PV}(k - 1)| > \epsilon$, where the proposed partial

shading algorithm is activated and searches for the new MPP, otherwise, if $|p_{PV}(k) - p_{PV}(k - 1)| < \epsilon$ only the modified P&O-VS algorithm is activated, saving tracking time by using only part of the proposed algorithm, FIGURE 10.

V. RESULTS

To show the proposed algorithm performance, simulations and experimental tests are performed. The simulations are obtained from the software PSIM 9.1, using switching-based model.

A. SIMULATED RESULTS

Four cases are studied, considering an array of three strings, as shown in FIGURE 9, one case contemplates USC and the three other cases PSC, *i.e.*, with and without partial shading respectively, as presented in FIGURE 12. The details for every case are shown in TABLE 2, highlighting the irradiance values, the power and voltage at the GMPP, and the temperature is kept constant to 20°C for all cases.

TABLE 2. Parameters of the study cases.

	Case 1	Case 2	Case 3	Case 4
String 1	700 [W/m ²]	700 [W/m ²]	700 [W/m ²]	700 [W/m ²]
String 2	700 [W/m ²]	420 [W/m ²]	420 [W/m ²]	70 [W/m ²]
String 3	700 [W/m ²]	420 [W/m ²]	210 [W/m ²]	70 [W/m ²]
P_{GMPP}	10754 [W]	6831 [W]	4687 [W]	3585 [W]
V_{GMPP}	1804 [V]	1870 [V]	1270 [V]	601 [V]

For the solar array illustrated in FIGURE 9, the GMPP voltage can be found around v_{Ns3} , v_{Ns2} , or v_{Ns1} ($N_s = 3, 2$, or 1), where the conditions to find the GMPP in around these voltages are listed in TABLE 2 and illustrated in FIGURE 12. Thus, if the system can reach the GMPP independent of three possible locations it may be, the algorithm can work in any climate condition. All four cases are detailed below:

Case 1: There is only one MPP, since the system is without shading.

Case 2: There are two points of maximum power (LMPP-GMPP), where two of the three strings have the same level of partial shading, with an irradiance gain of 0.6 for strings 2 and 3.

Case 3: There are three local maximum points (LMPP-GMPP-LMPP), where strings 2 and 3 have a gain of 0.6 and 0.3, respectively.

Case 4: The three strings are almost entirely shadowed, getting two points of maximum power (GMPP-LMPP), where string 2 and 3 have a gain of 0.1.

The simulation parameters of the PV system are presented in TABLE 3, an array of 60 PV panels divided into three strings in series is used, obtaining the results presented in FIGURE 13 and FIGURE 14. All controllers run in the same script, where the sampling frequency is $f_s = 10kHz$.

FIGURE 13 shows a simulation where the systems go through all cases: case 1, between 0-0.8s; case 2,

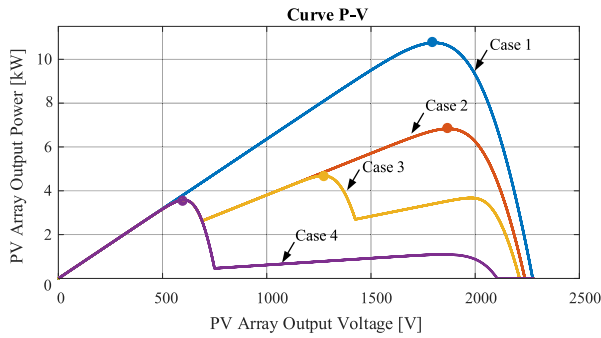


FIGURE 12. Curve P-V of the study cases.

TABLE 3. Simulation parameters.

Parameters		Value	
PV Array			
Number Panels in Serie N_p		20	
Number String in Serie N_s		3	
Number String in Paralel N_{sp}		1	
Maximum Power in USC $P_{MPP-array}$		15.9 [kW]	
Maximum Voltage in USC $V_{MPP-array}$		1854 [V]	
GMPPT Algorithm	Integrative Time for v_{oc1} T_i^1	$-5.25 \cdot 10^{-7}$	
	Integrative Time for v_{oc2} T_i^2	$2.766 \cdot 10^{-4}$	
DC-link Capacitor C_{dc}		1 [mF]	
Resistance Filter R		0.5 [Ω]	
Inductor Filter L		0.7 [mH]	
Source Voltage RMS v_s^{abc}		220 [V]	
Source Frequency f		50 [Hz]	
Switching Frequency f_{sw}		10.5 [kHz]	
Converter Parameters	PI v_{dc}	$k_c^{v_{dc}}$	0.0635
		$T_i^{v_{dc}}$	0.0158
	PI i_s^{dq}	$k_c^{i_s}$	1269
		$T_i^{i_s}$	0.0016

between 0.8-1.5s; case 3, between 1.5-2.2s; and case 4, between 2.2-2.8s. FIGURE 13 (a) shows the power behavior, obtaining the GMPP for all cases indicated in FIGURE 12. FIGURE 13 (b) shows the reference voltage from the proposed algorithm, this voltage will be explained in depth in FIGURE 14. FIGURE 13 (c) shows the variation voltage Δv used in the modified P&O-VS algorithm, where Δv starts from 10V decreasing at steps of 2V down to $\Delta v = 2V$, from this point forward the decrement will be 0.1V until reaching zero, which indicates that the MPP or GMPP was found. FIGURE 13 (d) variations of N_s of the proposed partial shading algorithm are presented, where each of the values is tested at the beginning, also when there is a change in power PV, the variation begins with the maximum number of strings ($N_s = 3$) and ends in one ($N_s = 1$). It is observed as for the case 1 and 2 $N_s = 3$ represents the GMPP, for the case 3 $N_s = 2$ is associated with the GMPP, and in case 4 $N_s = 1$ is associated to the GMPP, which is applied in (40) to determine the voltage (v_{dc}^{ref}) to work in the PV system. The tracking time for the cases analyzed is approximately 0.6s.

In FIGURE 14, a zoom of FIGURE 13-Case 1 on the proposed algorithm behavior is presented, also the injection

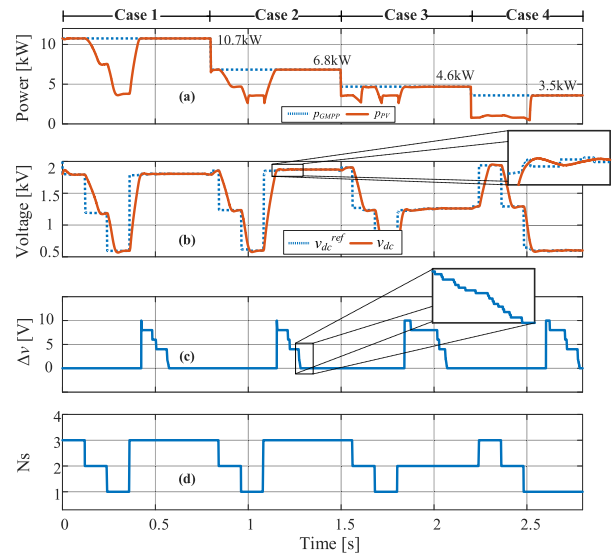


FIGURE 13. Simulated results for study cases. (a) Global maximum power point tracking (GMPPT), (b) PV array DC voltage V_{MPPT} (V_{dc}), (c) Voltage variation P&O-VS modified algorithm Δv , (d) String number test N_s .

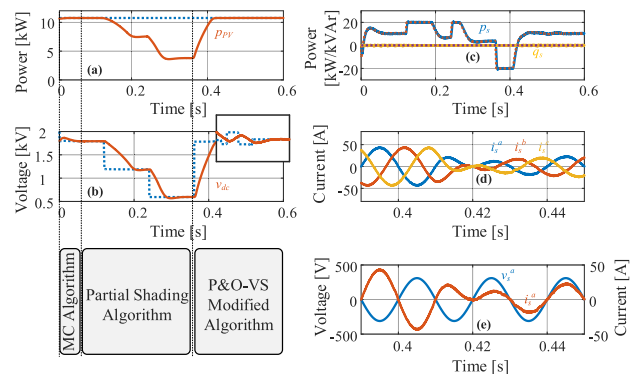


FIGURE 14. DC and AC behavior. (a) Global maximum power point tracking (GMPPT) from 0 to 0.6s, (b) PV Array DC voltage V_{MPPT} (V_{dc}) from 0 to 0.6s, (c) Active and reactive power from 0 to 0.6s, (d) AC current from 0.39 to 0.45s, (e) Voltage Source v_s^a vs current source i_s^a from 0.39 to 0.45s.

to the grid. FIGURE 14 (a), (b) show the behavior of the proposed algorithm, where in FIGURE 14 (b) between 0-0.04s the MC algorithm gives the initial voltage, then the proposed partial shading algorithm is enabled between 0.04-0.36s testing the values of N_s ($N_s = 3, 2, 1$), and finally, between 0.424-0.535s the proposed modified P&O-VS algorithm is enabled to get closer to the GMPP, and therefore, the final adjust given by the P&O-VS only takes 0.111s. FIGURE 14 (c) shows how the active power (p_s) and reactive power (q_s) follow their reference determined from the voltage control loop and the power factor ($pf = 1$). Furthermore, the power is limited to $\pm 20kW$ and therefore an anti-windup algorithm is required to avoid over-integration. FIGURE 14 (d) shows the three phase AC currents under PSC. In FIGURE 14 (e) the voltage v_s^a and current i_s^a can be seen with a phase-shift equal to zero degrees, tracking

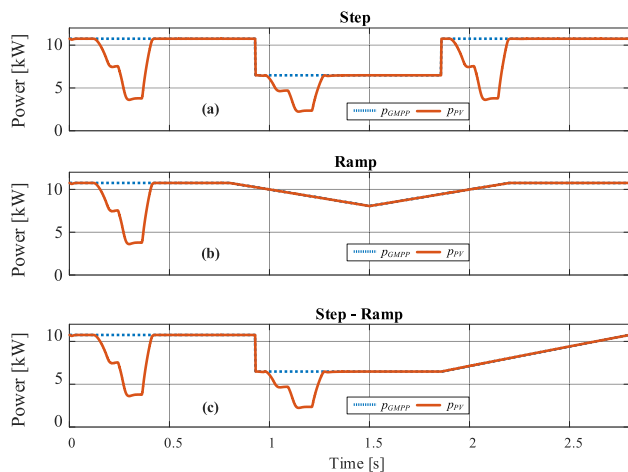


FIGURE 15. Maximum power point tracking at different irradiance variations. (a) Step, (b) Ramp, (c) Step-Ramp.

its reference of unitary power factor. Thus, from FIGURE 14 the algorithm proposed can be seen in detail.

Finally, to check the robustness of the algorithm, FIGURE 15 shows the behavior of the algorithm under step, ramp, and step-ramp variations of the irradiance. For all cases the changes were made equally to each string. In FIGURE 15 (a) a step change is made from 700W/m² to 420W/m² and then back to the initial value, obtaining the maximum power using the proposed algorithm. In FIGURE 15 (b) a ramp change is performed progressively from 700W/m² down to 520W/m² approximately, in this case it is observed that since the power variation is small ($|p_{PV}(k) - p_{PV}(k - 1)| < \epsilon$) only the P&O Modified Algorithm is used, without entering the stage of testing the N_s , which in this case is not necessary. FIGURE 15 (c) presents a combination of the previous cases under step change at 0.9s and a ramp change at 1.8s, it is observed that since the power variation is large (4kW) the algorithm tests the N_s , and then, before the ramp changes, only the P&O Modified Algorithm is used.

B. EXPERIMENTAL RESULTS

The Experimental results are obtained using a PV array of 5 panels in series with bypass diode, a voltage source inverter, a RL filter, a resistive load, a Programmable Source CSW5550 from California Instruments, and the TMS320F28335 DSC based board, as shown in FIGURE 16 the resistive load is used since the programable source is not regenerative and the power due to the solar array needs to be consumed. The experimental parameters are listed in TABLE 4.

To validate the proposed algorithm, it is necessary the measurement of v_{oc} and i_{sc} of the solar cell, to obtain these measurements there are two possibilities:

- i) online, measuring at all times the v_{oc} and i_{sc} parameters, which leads to a more accurate v_{MPP} .
- ii) off-line, in case of not having two PV cells from the same manufacturer of the PV array, measure only once the

TABLE 4. Experimental parameters.

Parameters		Value
PV Panel	Power max p_{MPP}	10 [W]
	Open Circuit Voltage v_{oc}	21.6 [V]
	Short Circuit Current i_{sc}	0.61 [A]
	Maximum Power Voltage v_{MPP}	17.8 [V]
	Maximum Power Current i_{MPP}	0.56 [A]
Converter Parameters	DC-link Capacitor C_{dc}	2.35 [mF]
	Resistance Filter R	0.5 [Ω]
	Inductor Filter L	12 [mH]
	Source Voltage RMS v_s^{abc}	13 [V]
	Source Frequency f	50 [Hz]
	Switching Frequency f_{sw}	≈ 9.25 [kHz]

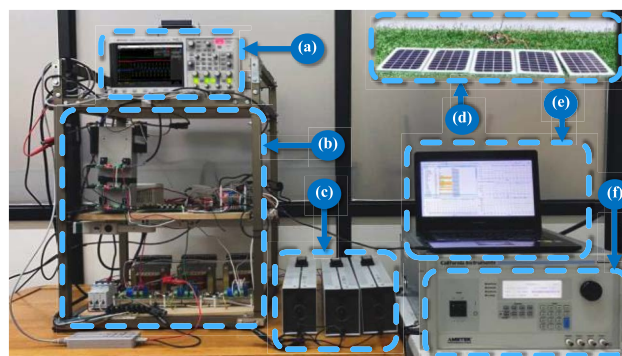


FIGURE 16. Experimental configuration for testing the proposal algorithm. (a) Oscilloscope, (b) Voltage source inverter - Inductor - Sensors - Conditioning circuit - DSC, (c) Resistive load, (d) PV array, (e) Laptop for programming the DSC, (f) Three phase AC programming source.

v_{oc} and i_{sc} parameters from a PV panel of the array may lead to obtaining a not so accurate v_{MPP} but, thanks to the modified P&O-VS algorithm, the GMPP is correctly obtained.

Therefore, the off-line method is used to obtain the values of v_{oc} and i_{sc} from one panel of the PV array containing 36 cells. The results showed $v_{oc} = 20.16V/36 = 0.56V$ and $i_{sc} = 0.484A$ at the time of experimentation, where the ambient temperature was about 20°C and the irradiance was 750 [W/m²]. The latter value is determined using the i_{sc} value and the expression,

$$S_{PV} = \frac{S_0}{I_{sc0}} i_{sc}. \tag{41}$$

where $S_0 = 1000$ [W/m²] is the standard intensity of the irradiancy, $I_{sc0} = 0.61A$ is the short circuit current of the solar cell at the standard conditions, and i_{sc} is the short circuit current measured.

The experimental results are shown in FIGURE 17, FIGURE 18, and FIGURE 19 for a PSC system. The parameters of the modified P&O-VS are: $\Delta Max = 2$, $\Delta Min = 1$, $\delta v = 0.1$. FIGURE 17 shows the results considering only one solar panel shaded, so N_s must change from 3 to 2. The power p_{PV} , voltage v_{dc} and the current i_{dc} are shown in FIGURE 17 (a), where it is observed as v_{dc} changes based on the N_s values ($N_s = 3, 2, 1$), finding the global voltage in the maximum power point (v_{GMPP}) with $N_s = 2$ ($v_{GMPP} \approx 65V$). Once N_s is chosen, then it is enabled the modified P&O-VS

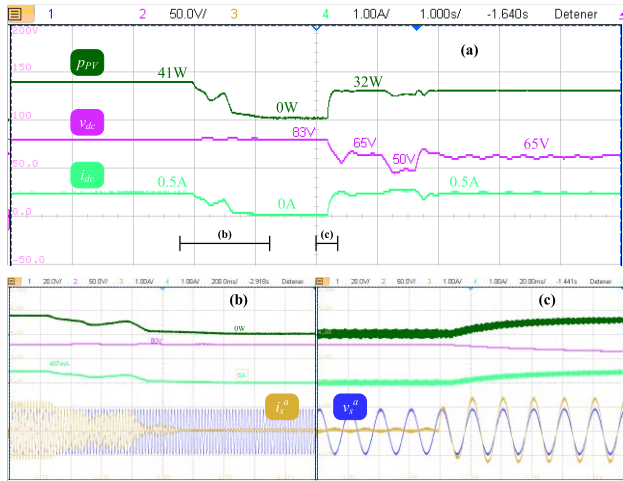


FIGURE 17. Experimental results oscilloscope, shaded a single PV panel, change $N_s = 3$ to $N_s = 2$. (a) DC variables: power p_{PV} , voltage v_{dc} , and current i_{dc} . (b) Zoom when panel is shaded, DC and AC variables, (c) Zoom when the proposed partial shading algorithm is enabled, DC and AC variables.

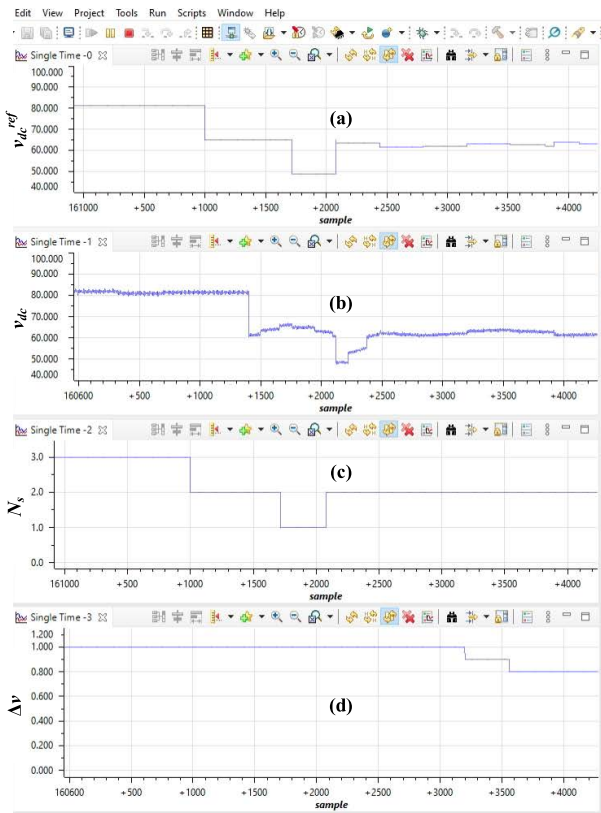


FIGURE 18. Experimental result from CCS. (a) Reference voltage v_{dc}^{ref} , (b) Voltage v_{dc} , (c) String number test N_s , (d) Voltage variation P&O-VS modified algorithm Δv .

algorithm, to get closer to the GMPP. FIGURE 17 (b) shows the moment when one of the PV panels is shaded, the voltage is maintained ($v_{dc} = 83V$) but the current drops to 0A, as well as the PV power ($p_{PV} = 0$), causing a power variation which would enable the partial shading algorithm,

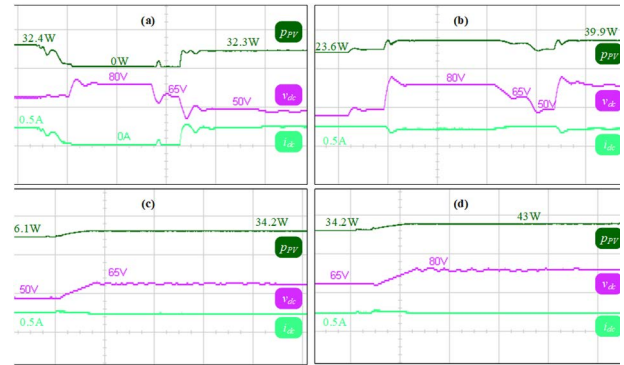


FIGURE 19. Experimental results for different types of partial shading. Obtaining: (a) $N_s = 2$ to $N_s = 1$, (b) $N_s = 1$ to $N_s = 3$, (c) $N_s = 1$ to $N_s = 2$, (d) $N_s = 2$ to $N_s = 3$.

increasing the power when the voltage v_{dc} decreases as shown in FIGURE 17 (c). Additionally, it can be seen a unitary power factor at the AC side.

FIGURE 18 presents the results in the software Code Composer Studio (CCS). Particularly, FIGURE 18 (a) shows the voltage v_{dc}^{ref} reference, FIGURE 18 (b) shows the actual v_{dc} voltage, allowing to see the voltage dynamic, FIGURE 18 (c) highlights the moment when the partial shading algorithm is enabled, changing N_s from 3 to 1, obtaining the GMPP for $N_s = 2$. Then, once the partial shading algorithm is finished, the modified P&O-VS is enabled, decreasing the voltage variation Δv , as follows in FIGURE 18 (d).

Finally, the FIGURE 19 presents the different tests of the PV system with partial shading, changing $N_s = 2$ to $N_s = 1$ in FIGURE 19 (a), $N_s = 1$ to $N_s = 3$ in FIGURE 19 (b), $N_s = 1$ to $N_s = 2$ in FIGURE 19 (c), and $N_s = 2$ to $N_s = 3$ in FIGURE 19 (d). Nevertheless, in FIGURE 19 (c) and FIGURE 19 (d), the voltage variations are made only with modified P&O-VS algorithm, without using the partial shading algorithm, since, $|p(k) - p(k - 1)| < \epsilon$ (the power variation is low), only the modified P&O-VS algorithm is used to find the v_{GMPP} .

VI. CONCLUSION

It is proposed to employ a three-phase VSC with a nonlinear based control strategy for the supply currents and a linear PI controller for the DC-link voltage to inject the power into the grid from a PV system. The PVs could be exposed to partial shading and the GMPPT is obtained using a combination of two algorithms, the MC and the P&O. The combination of these two algorithms allows to rapidly find the surrounding of the MPP by the MC method, and then, the modified P&O method is employed to improve the approximation to the GMPP. The modified P&O algorithm reduces its voltage step as it gets closer to the MPP; therefore, it reduces the oscillations around the MPP, thus, reducing the DC-link voltage reference noise and consequently the current reference noise. The MPPT algorithm wakes up only when the power changes its values from the steady state one, leading to supply a steady power to grid. The proposed MPPT is tested under several

circumstances, proving that under extreme simulated and realistic experimental tests can reach the GMPP by employing the proposed strategy.

REFERENCES

- [1] *Future of Wind: Deployment, Investment, Technology, Grid Integration and Socio-Economic Aspects*, IRENA, Abu Dhabi, United Arab Emirates, 2019.
- [2] M. Malinowski, J. I. Leon, and H. Abu-Rub, "Solar photovoltaic and thermal energy systems: Current technology and future trends," *Proc. IEEE*, vol. 105, no. 11, pp. 2132–2146, Nov. 2017.
- [3] R. B. Bollipo, S. Mikkili, and Y. P. K. Bonthagorla, "Hybrid, optimal, intelligent and classical PV MPPT techniques: A review," *CSEE J. Power Energy Syst.*, vol. 7, no. 1, pp. 9–33, Jan. 2021.
- [4] R. Motamarrri and B. Nagu, "GMPPT by using PSO based on Lévy flight for photovoltaic system under partial shading conditions," *IET Renew. Power Gener.*, vol. 14, no. 7, pp. 1143–1155, 2020.
- [5] A. Ali, K. Almutairi, S. Padmanaban, V. Tirth, S. Algarni, K. Irshad, S. Islam, M. H. Zahir, M. Shafiullah, and M. Z. Malik, "Investigation of mppt techniques under uniform and non-uniform solar irradiation condition-a retrospection," *IEEE Access*, vol. 8, pp. 127368–127392, 2020.
- [6] S.-C. Wang, H.-Y. Pai, G.-J. Chen, and Y.-H. Liu, "A fast and efficient maximum power tracking combining simplified state estimation with adaptive perturb and observe," *IEEE Access*, vol. 8, pp. 155319–155328, 2020.
- [7] A. M. Eltamaly, M. S. Al-Saud, and A. G. Abokhalil, "A novel bat algorithm strategy for maximum power point tracker of photovoltaic energy systems under dynamic partial shading," *IEEE Access*, vol. 8, pp. 10048–10060, 2020.
- [8] D. Yousri, T. S. Babu, E. Beshr, M. B. Eteiba, and D. Allam, "A robust strategy based on marine predators algorithm for large scale photovoltaic array reconfiguration to mitigate the partial shading effect on the performance of PV system," *IEEE Access*, vol. 8, pp. 112407–112426, 2020.
- [9] D. R. Espinoza Trejo, S. Taheri, J. L. Saavedra, P. Vazquez, C. H. De Angelo, and J. A. Pecina-Sanchez, "Nonlinear control and internal stability analysis of series-connected boost DC/DC converters in PV systems with distributed MPPT," *IEEE J. Photovolt.*, vol. 11, no. 2, pp. 504–512, Mar. 2021.
- [10] C. Rao, A. Hajjiah, M. A. El-Meligy, M. Sharaf, A. T. Soliman, and M. A. Mohamed, "A novel high-gain soft-switching DC–DC converter with improved P&O MPPT for photovoltaic applications," *IEEE Access*, vol. 9, pp. 58790–58806, 2021.
- [11] S. Mohanty, B. Subudhi, and P. K. Ray, "A new MPPT design using grey wolf optimization technique for photovoltaic system under partial shading conditions," *IEEE Trans. Sustain. Energy*, vol. 7, no. 1, pp. 181–188, Jan. 2016.
- [12] C. Huang, L. Wang, Z. Zhang, R. Shun-Cheung Yeung, A. Bensoussan, and H. Shu-Hung Chung, "A novel spline model guided maximum power point tracking method for photovoltaic systems," *IEEE Trans. Sustain. Energy*, vol. 11, no. 3, pp. 1309–1322, Jul. 2020.
- [13] K. Guo, L. Cui, M. Mao, L. Zhou, and Q. Zhang, "An improved gray wolf optimizer MPPT algorithm for PV system with FBFC converter under partial shading," *IEEE Access*, vol. 8, pp. 103476–103490, 2020.
- [14] H. Li, D. Yang, W. Su, J. Lü, and X. Yu, "An overall distribution particle swarm optimization MPPT algorithm for photovoltaic system under partial shading," *IEEE Trans. Ind. Electron.*, vol. 66, no. 1, pp. 265–275, Jan. 2019.
- [15] Y. Wang, Y. Li, and X. Ruan, "High-accuracy and fast-speed MPPT methods for PV string under partially shaded conditions," *IEEE Trans. Ind. Electron.*, vol. 63, no. 1, pp. 235–245, Jan. 2016.
- [16] S. Selvakumar, M. Madhusmita, C. Koodalsamy, S. P. Simon, and Y. R. Sood, "High-speed maximum power point tracking module for PV systems," *IEEE Trans. Ind. Electron.*, vol. 66, no. 2, pp. 1119–1129, Feb. 2019.
- [17] J. Saikrishna Goud, R. Kalpana, and B. Singh, "A hybrid global maximum power point tracking technique with fast convergence speed for partial-shaded PV systems," *IEEE Trans. Ind. Appl.*, vol. 54, no. 5, pp. 5367–5376, Oct. 2018.
- [18] Q. Wang, K. Jaffres-Runser, Y. Xu, J.-L. Scharbarg, Z. An, and C. Fraboul, "TDMA versus CSMA/CA for wireless multihop communications: A stochastic worst-case delay analysis," *IEEE Trans. Ind. Informat.*, vol. 13, no. 2, pp. 877–887, Apr. 2017.
- [19] R. Morales, M. Garbarino, J. Muñoz, J. Rohten, V. Esparza, and D. Dewar, "Grid connected PV system with new MPPT estimation method based on measuring cells," in *Proc. 45th Annu. Conf. IEEE Ind. Electron. Soc.*, Oct. 2019, pp. 2366–2371.
- [20] J. Silva, J. Espinoza, M. Torres, J. Rohten, C. Baier, and J. Muñoz, "Global maximum power point tracking scheme on a partially shaded photovoltaic array," in *Proc. 44th Annu. Conf. IEEE Ind. Electron. Soc. (IECON)*, Oct. 2018, pp. 1830–1834.
- [21] J. Silva, J. Espinoza, J. Rohten, M. Torres, and E. Espinosa, "Grid connected PV system with maximum power point estimation based on reference cells," in *Proc. 41st Annu. Conf. IEEE Ind. Electron. Soc. (IECON)*, Nov. 2015, pp. 4070–4075.
- [22] M. A. Hannan, I. Hussin, P. J. Ker, and M. M. Hoque, "Advanced control strategies of VSC based HVDC transmission system: Issues and potential recommendations," *IEEE Access*, vol. 6, pp. 78352–78369, 2018.
- [23] S. Kouro, J. I. Leon, D. Vinnikov, and L. G. Franquelo, "Grid-connected photovoltaic systems: An overview of recent research and emerging PV converter technology," *IEEE Ind. Electron. Mag.*, vol. 9, no. 1, pp. 47–61, Mar. 2015.
- [24] J. A. Rohten, D. N. Dewar, P. Zanchetta, and A. Formentini, "Multivariable deadbeat control of power electronics converters with fast dynamic response and fixed switching frequency," *Energies*, vol. 14, no. 2, p. 313, 2021.
- [25] J. A. Rohten, J. E. Muñoz, E. S. Pulido, J. J. Silva, F. A. Villarroel, and Y. J. R. Espinoza, "Very low sampling frequency model predictive control for power converters in the medium and high-power range applications," *Energies*, vol. 14, no. 1, p. 199, 2021.
- [26] J. A. Rohten, J. J. Silva, J. A. Munoz, F. A. Villarroel, D. N. Dewar, M. E. Rivera, and J. R. Espinoza, "A simple self-tuning resonant control approach for power converters connected to micro-grids with distorted voltage conditions," *IEEE Access*, vol. 8, pp. 216018–216028, 2020.
- [27] P. Zambrana, J. Fernandez-Quijano, J. J. Fernandez-Lozano, P. M. M. Rubio, and Y. A. J. Garcia-Cerezo, "Improving the performance of controllers for wind turbines on semi-submersible offshore platforms: Fuzzy supervisor control," *Energies*, vol. 14, no. 19, p. 6222, Sep. 2021.
- [28] C. Huang, D. Yue, X. Xie, and Y. J. Xie, "Anti-windup load frequency controller design for multi-area power system with generation rate constraint," *Energies*, vol. 9, no. 5, p. 330, Apr. 2016.
- [29] S. Dormido, "Advanced PID control—[Book review]," *IEEE Control Syst.*, vol. 26, no. 1, pp. 98–101, Feb. 2006, doi: 10.1109/MCS.2006.1580160.
- [30] J. R. Espinoza, G. Joos, and L. Moran, "Decoupled control of the active and reactive power in three-phase PWM rectifiers based on non-linear control strategies," in *Proc. 30th Annu. IEEE Power Electron. Spec. Conf. Rec.*, vol. 1, Jul. 1999, pp. 131–136.
- [31] J. A. Rohten, J. R. Espinoza, J. A. Muñoz, P. E. Melín, and E. E. Espinosa, "Discrete nonlinear control based on a double dq transform of a multi-cell UPQC," in *Proc. 37th Annu. Conf. IEEE Ind. Electron. Soc. (IECON)*, Nov. 2011, pp. 4134–4139.
- [32] P. Henriquez, S. Cuevas, J. Rohten, S. Araya, V. Esparza, G. Sanhueza, and P. Melin, "Nonlinear control for power converters injecting the maximum power from PV arrays," in *Proc. IEEE Int. Conf. Automatica (ICA-ACCA)*, Oct. 2016, pp. 1–6.
- [33] R. Morales, M. Garbarino, J. Rohten, J. Muñoz, V. Esparza, and Y. E. Rubio, "Maximum power point tracking algorithms comparison for three-phase power converter," in *Proc. IEEE CHILEAN Conf. Elect., Electron. Eng., Inf. Commun. Technol. (CHILECON)*, Nov. 2019, pp. 1–7.
- [34] F. Paz and M. Ordóñez, "Zero oscillation and irradiance slope tracking for photovoltaic MPPT," *IEEE Trans. Ind. Electron.*, vol. 61, no. 11, pp. 6138–6147, Nov. 2014.



RODRIGO H. MORALES received the degree in automation engineering from the Universidad del Bío-Bío, Concepción, Chile, in 2018, and the master's degree from the Universidad de Talca, in 2022. He is currently pursuing the D.Sc. degree with the Universidad de Concepción. Since 2019, he has been teaching with the Department of Electrical and Electronic Engineering, Universidad del Bío-Bío. His research interests include renewable energies and PV systems for voltage source converters.



JAIME A. ROHTEN (Member, IEEE) received the Engineering degree (Hons.) in electronic engineering and the M.Sc. and D.Sc. degrees in electrical engineering from the University of Concepcion, Concepción, Chile, in 2010, 2012, and 2017, respectively. Since 2015, he has been teaching in the areas of power electronic and control systems analysis with the Department of Electrical and Electronic Engineering, Universidad del Bío-Bío, Concepción. His research interests include renewable energies, digital nonlinear, and resonant and predictive control for voltage or current source converters.



MATÍAS N. GARBARINO received the degree in automation engineering from the Universidad del Bío-Bío, Concepción, Chile, in 2018, and the master's degree from the Universidad de Talca, in 2022. He is currently pursuing the D.Sc. degree with the Universidad de Concepción. Since 2019, he has been teaching control systems at the Laboratory of Universidad del Bío-Bío, and INACAP, Concepción. His research interests include renewable energies, systems control, and electric power conversion.



JAVIER A. MUÑOZ (Member, IEEE) was born in Concepción, Chile, in 1983. He received the B.S. (Hons.), M.Sc., and D.Sc. degrees in electrical engineering from the University of Concepcion, Concepción, in 2007, 2009, and 2012, respectively. Since April 2011, he has been with the Department of Industrial Technologies, University of Talca, Curicó, Chile, where he is currently teaching in the areas of dynamic systems and robotics. His research interest includes digital control of modular multi-level converters to improve power quality.



JOSÉ J. SILVA received the Engineering degree (Hons.) in electronic engineering and the M.Sc. and Ph.D. degrees in electrical engineering from the Universidad de Concepción, Concepción, Chile, in 2014, 2015, and 2021, respectively. Since 2015, he has been teaching in the area of control and electricity. He is currently an Associate Professor at the Universidad de Los Lagos, teaching the subjects of electrical machines and electrical drives. His research interests include weak grids, wind systems, photovoltaic systems operating in partial shadow conditions, digital control, multilevel converters, model predictive control, and control of electrical machines.



ESTEBAN S. PULIDO received the B.S. and M.Sc. degrees in electrical engineering from the Universidad Técnica Federico Santa María (UTFSM), Valparaíso, Chile, in 2002 and 2006, respectively, and the D.Sc. degree in electrical engineering from the Universidad de Concepción, Concepción, Chile, in 2021.

He was a Power System Analyst and an Engineer Operation and Planning at Trans-elec transmission company, Santiago, Chile, from 2006 to 2012. Since 2013, he has been a Professor with the Department of Electrical Engineering, UTFSM. His main research interests include the power protection systems, power systems transients, and the integration of renewable energy systems.



JOSE R. ESPINOZA (Senior Member, IEEE) received the Engineering degree in electronic engineering and the M.Sc. degree in electrical engineering from the University of Concepción, Concepción, Chile, in 1989 and 1992, respectively, and the Ph.D. degree in electrical engineering from Concordia University, Montreal, QC, Canada, in 1997. Since 2006, he has been a Professor with the Department of Electrical Engineering, University of Concepción, where he is engaged in

teaching and research in the areas of automatic control and power electronics. He has authored or coauthored more than 250 refereed journals and conference papers and contributed to one chapter in the *Power Electronics Handbook* published in 2011 by Academic Press. He is currently an Associate Editor of the IEEE TRANSACTIONS ON POWER ELECTRONICS and the IEEE TRANSACTIONS ON INDUSTRIAL INFORMATICS.



MARCOS L. ANDREU received the Engineering degree in automation engineering from the Universidad del Bío-Bío, Concepción, Chile, in 2019, and the M.Sc. degree in electrical engineering from the University of Concepción. He is currently pursuing the Ph.D. degree with the University of Arizona. Since 2019, he has been teaching in the area of automation and robotics at INACAP. His research interests include power converter control, specifically classical, nonlinear, and robust control for renewable energies applications.

...